Engineering Failure Analysis 105 (2019) 597–609

Contents lists available at ScienceDirect

Engineering Failure Analysis

journal homepage: www.elsevier.com/locate/engfailanal

Effect of low temperatures on constant amplitude fatigue properties of Q345qD steel butt-welded joints

Xiaowei Liao[a,b], Yuanqing Wang[b], Zongyi Wang[b,*], Liuyang Feng[c], Yongjiu Shi[b]

[a] College of Civil Engineering and Architecture, Zhejiang University of Technology, Hangzhou 310023, China
[b] Department of Civil Engineering, Tsinghua University, Beijing 100084, China
[c] Department of Civil and Environmental Engineering, National University of Singapore, Singapore 117576, Singapore

ARTICLE INFO

Keywords:
Fatigue test
Low temperature
Butt-welded joint
Bridge steel Q345qD
Crack propagation analysis

ABSTRACT

The development of transportation infrastructures stimulates increasingly more welded steel bridges in cold and severe cold regions in China. The low temperature there imposes additional challenges for the welded fatigue details. This study firstly examines experimentally the fatigue properties of the butt-welded joints made of Q345qD bridge steel under high-cycle constant-amplitude tensile action at the room and low temperature of −60 °C. The experimental results reveal the occurrence of multiple fatigue crack initiation and illustrate that the low temperature increases slightly the fatigue strength of the butt-welded details. The numerical simulation examines the fatigue crack propagation behavior of butt-welded joints with initial pre-existing single and multiple cracks under the room and low temperature, which achieves a good agreement with the experimental results. Based on the experimental and numerical validation, this study finally discusses the effect of the low temperature on the fatigue life of butt-welded joints and demonstrates that the lower fracture toughness under the low ambient temperatures influences marginally on the fatigue crack propagation life of the butt-welded details. The enhanced resistance to the fatigue crack propagation of structural steels at low temperatures contributes to the improved fatigue strengths of the butt-welded joints.

1. Introduction

The butt-welded joints in steel bridges and offshore structures often are subjected to fatigue issues caused by the cyclic actions, which create great threats to the safety of these structures. In China, the cold and sever cold regions have almost occupied 60% of the whole mainland, and the lowest temperature reaches −54 °C [1]. The increasingly demand of steel bridges in those cold areas implies that the fatigue behavior of the welded joints under the low temperature is critical. A better understanding of the low-temperature fatigue behavior of welded details facilitates the design of new steel bridges and assessment of bridges in service. However, in comparison with detailed design specification in standards [2–4] and extensive fatigue research work [5–8] under the room temperature (RT), the fatigue properties of welded plate joints under the low temperatures requires further detailed experimental and numerical investigations.

Previous research efforts [9–12] have demonstrated that the reduced temperature usually increases the yield and ultimate tensile strength of structural steels, enhances the resistance to fatigue crack propagation but reduces their impact toughness and fracture toughness indices. Stephens [9] has indicated that the low-temperature fatigue properties of notched specimens become more

* Corresponding author at: Department of Civil Engineering, Tsinghua University, Beijing 100084, China.
E-mail address: wangzongyi1990@outlook.com (Z. Wang).

https://doi.org/10.1016/j.engfailanal.2019.07.006
Received 12 May 2019; Received in revised form 28 June 2019; Accepted 1 July 2019
Available online 02 July 2019
1350-6307/

Nomenclature

a = crack depth
a_0 = initial crack depth
a_{cr} = critical crack depth
a_g = distance between initial semi-elliptical crack centers
a_p = position of initial semi-elliptical crack center
Δa_i = increment of crack length for crack front node i
A_{KV} = Charpy impact energy
c = half of crack width
h_1, h_2 = height of the weld bead
K_I = Mode-I stress intensity factor
K_{IC} = fracture toughness of steel material
$K_{I,max}$ = Maximum mode-I stress intensity factor under cyclic loading
ΔK_I, ΔK_{II}, ΔK_{III} = Mode-I, II, and III stress intensity factor range
ΔK_{eq} = equivalent stress intensity factor range
N = number of loading cycles
R_i = stress ratio of applied cyclic load at node i
w_1, w_2 = width of the butt weld
W = width of the effective segment in butt-welded joint specimen
t = main plate thickness of butt-welded joint specimen
σ_{max} = applied maximum tensile stress
$\Delta\sigma$ = stress range
$\Delta\sigma_C$ = fatigue strength at 2 million cycles
υ = Poisson ratio

sensitive to the stress concentration. Jia & Liu [13] have carried out the fatigue tests of butt-welded joints and cruciform fillet-welded joints made of ASTM A131 steel at −25 °C, and collected the low-temperature S–N curves of those joints. Shul'ginov & Matveyev [14] have experimentally demonstrated that at low temperatures, the fatigue strength under sinusoidal loading increase but decrease under the impact loading for butt-welded joints made of low-alloy steels. Kang et al. [15] has concluded that the welding process has a determined effect on the fatigue life of butt-welded SM490A steel joints, in contrast to negligible effects due to the low temperature. Jeong et al. [16] presented that the butt-welded joints of Fe15Mn steel at −163 °C exhibited a greater resistance to the S–N fatigue than that at RT. Based on the above limited studies, there are controversial conclusions about the fatigue behavior of butt-welded joints under the low temperature, especially for the butt-welded joints fabricated with bridge steels.

In addition, the fatigue crack propagation life accounts for a major portion of the total fatigue life in as-welded joints with inherent cracks or crack-like defects. Therefore, the linear-elastic fracture mechanics (LEFM) is applicable to predict the crack propagation life of the welded joints. Bowness & Lee [17] and Lie et al. [18] have developed the formula solutions of mode-I stress intensity factor(SIF) K_I for the fatigue life prediction. Nykänen et al. [19] and Barsoum & Jonsson [20] have utilized the 2D cracked finite element (FE) model to facilitate the calculation of the K_I. Recently, the 3D crack propagation analysis of welded details has increasingly attracted more attentions [7,21–24], which focuses on the mixed-mode(K_I + K_{II} + K_{III}) crack propagation simulation. Compared with the commonly-used formula solution and 2D FE analysis, this more refined 3D crack propagation analysis is more realistic and accurate. However, the 3D crack simulation lacks extensive validation and anticipates more research efforts.

This study aims to investigate the effect of the low temperature on the fatigue properties of butt-welded joints made of Q345qD

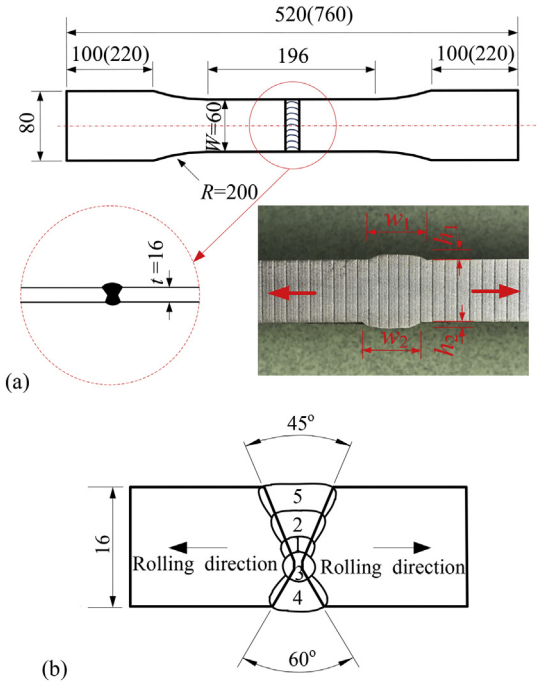

Fig. 1. Configuration of the butt-welded specimen (a) geometric dimension, (b) welding process (Unit: mm).

bridge steel, based on the fatigue experimental tests and numerical simulation of 3D crack propagation. Firstly, this study conducted a series of fatigue tests of butt-welded joint specimens at RT and −60 °C. Thereafter, this study simulated the refined 3D crack propagation analysis with single crack and multiple cracks based on the crack information obtained from fatigue tests and furthermore predicted the fatigue life of the butt-welded joints. The good achievement between test results and numerical prediction improved the understanding of the effect mechanism caused by the low temperature environment, and validated the accuracy and effectiveness of the 3D crack propagation analyses.

2. Material and experimental details

2.1. Materials and specimens

This study targets to conduct the high-cycle constant-amplitude fatigue test of butt-welded joints at RT and −60 °C. Fig. 1(a) presents the geometric dimensions and physic configuration of the fatigue specimens. The main plate thickness (t) is 15.5 mm, and the width (W) of the effective segment in the specimens is equal to 60 mm. Except for the values in brackets, which are the increased lengths of clamping ends and the specimens only for tests at −60 °C, the other geometric dimensions for the RT and low-temperature specimens are identical. The appearance quality satisfies the requirements in Chinese Code GB 50661 [25]. This plate-shaped joint includes two pieces of Q345qD steel plate and a double V-groove weld, using the multi-pass manual flux-cored arc welding(FCAW) process with filler metal E501T-1L. Fig. 1(b) illustrates the welding condition of the manual FCAW.

The Q345qD bridge steel is one of the most widely-used structural steels in bridges in China. The welding wire E501T-1L satisfies the strength requirements and exhibits a better impact toughness at low temperatures [26]. All the test specimens machined from the larger built-up test plates using wire cut technique guarantees the geometric and welding similarity. The yield strengths at RT and −60 °C of the Q345qD steel are 382 MPa and 429 MPa, while those of its butt weld are 580 MPa and 638 MPa respectively. The elastic modulus of both base and weld materials is averagely 209 GPa according to the uniaxial tensile tests [26].

2.2. Test procedure

Prior to the fatigue test, this study adopted a vernier caliper to measure the width of the butt welds and the height of the weld beads, as shown in Fig. 1(a). The measurement data provides more accurate dimension for the FE modeling of the butt-welded joint specimens.

The tests adopted constant-amplitude tensile loading with a sinusoidal waveform at a frequency of 4 Hz, using a MTS 810 servo-hydraulic testing machine with a dynamic capacity of ± 500 kN. An insulated chamber equipped with an automatic temperature control system guaranteed a stable and reliable low temperature ambient. The temperature around the specimens was real-time

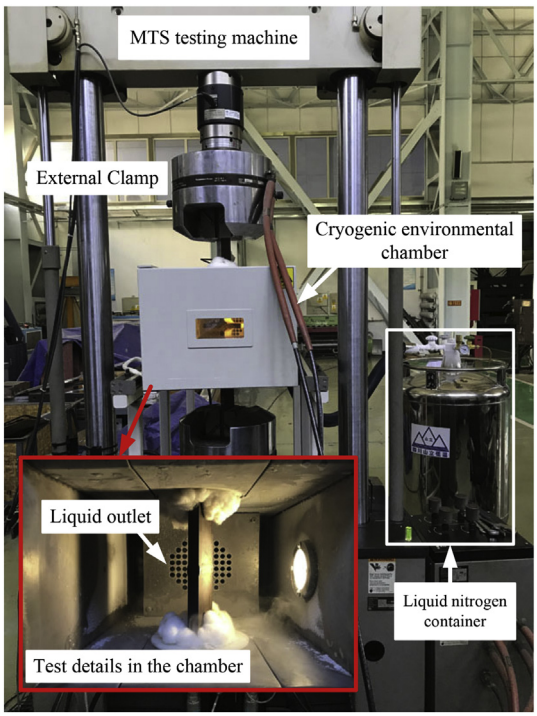

Fig. 2. Fatigue test setup at low temperatures.

monitored with a thermocouple. The feedbacks by the thermocouple intelligently kept the fluctuation amplitude of the testing temperature within ± 2 °C, by controlling the pumping rate of the liquid nitrogen into the chamber. Fig. 2 photographs the experimental setup at low temperatures. The fatigue tests include eight stress ranges with the stress ratio of 0.1. The maximum 2 million loading cycles or the occurrence of fatigue fracture of the specimens define a test termination.

Due to the cost limitation, the tests can harvest only one effective data under each stress range condition. Consequently, the fatigue test program collected 10 fatigued specimens at RT and 11 fatigued specimens at −60 °C. Finally, the macroscopic observation on the fractured surface of the fatigued specimens revealed the fatigue crack propagation morphology, which provided more accurate crack information for the 3D crack propagation numerical analysis.

3. Results

3.1. Geometry measurements

Table 1 statistically evaluates the values of the local geometric properties of the as-welded joints without differentiating the RT and low-temperature specimens. The mean values of the butt-weld width on the wider (w_1) and narrower sides (w_2) are 14.99 mm and 14.25 mm, respectively. The heights of the double-side weld beads (h_1, h_2) are less than 1.5 mm, which conforms to the requirements of code GB 50661 [25]. Benefitting from the strictly control of the welding processes, the axial misalignments were too small to be measured. According to the grouping criterion of fatigue details in Eurocode3 [3], the fatigue strength of this batch of butt-welded joints can be classified as FAT90.

3.2. Fracture surface of fatigued specimens

For the butt-welded joints at both RT and −60 °C, the fatigue cracks always originated at weld toes in the base plate, and then propagated also along the welds in base materials, perpendicular to the applied loads. Table 2 summarizes the crack types of the all fatigued specimens, and Fig. 3 macroscopically pictures some typical crack propagation configurations in the fracture surfaces of specimens fatigued at RT and −60 °C. The failure modes for the crack propagation primarily include single semi-elliptical cracks and multiple semi-elliptical cracks. This study also finds the cracks in the majority of specimens actually initiated and propagated simultaneously at several sites along the weld toes, as shown in Fig. 3(b) and (d).

In the fatigued specimens BW-7 and BW-9, this study observed the entire beach marks in the form of semi-elliptical cracks. The application of a dye penetrant along the weld toes at fixed time interval formed the beach marks on the fatigued specimen at RT, while the environmental chamber outside the fatigued specimens hindered the operation of dye penetration at −60 °C. Fig. 4(a) shows the crack aspect ratios (a/c) for some fatigued specimens as a function of the normalized crack depths (a/t) by plate thickness, including specimens BW-7, BW-9, BWL-2, BWL-7 and BWL-8. Measurement of the semi-elliptical beach marks derived the values of crack depth a and half of crack width c. Since the vibration amplitude of the observed a/c versus the crack depth is almost within the range of 0.6 to 0.8, this study adopts the mean values. The mean values a/c of tested specimens are about 0.7 at RT and 0.6 at −60 °C, which will be adopted as the initial crack aspect ratio in the later numerical analyses. Both of the observation values a/c are higher than the recommended initial value $a/c = 0.2$ by International Institute of Welding(IIW) [27]. However, results in previous researches [23,28,29] have presented that the values a/c negligibly affect the computed fatigue crack propagation life.

For the fractured specimens with the single semi-elliptical crack, Fig. 4(b) summarizes the critical crack depth normalized by the plate thickness of the fatigued specimens (a_{cr}/t) as a function of the center position of the semi-elliptical crack normalized by the plate width (a_p/W). The mean values of a_{cr}/t are 0.74 at RT and 0.72 at −60 °C. a_{cr} represents the critical crack depth, and a_p denotes the center position of the initial semi-elliptical crack.

3.3. Fatigue strength of butt-welded joints

Table 2 summarizes the fatigue test results of butt-welded joint specimens at RT and −60 °C. Fig. 5 plots the S–N fatigue data in the log-log logarithmic scale. All of the fatigue data points in this study locate above the FAT90 S–N curves in Eurocode3 [3], demonstrating that the specimens exhibit excellent welding qualities. Based on the best linear fitting of the test data, which regards the stress range log(Δσ) as the independent variable, this study derives the mean S–N curves ($\log N = \log C\text{-}m\log(\Delta\sigma)$) at RT and −60 °C. The fatigue strengths at 2 million cycles for specimens at RT and −60 °C are 134 MPa and 148 MPa, respectively. As the slopes of the two fitting S–N curves show insignificant difference, the mean S–N curve at −60 °C is almost above that at RT.

Table 1
Measured local dimensions of butt-welded joint specimens (Unit: mm).

Item	Dimensions of the butt weld			
	w_1	h_1	w_2	h_2
Mean value	14.99	1.23	14.25	1.16
Standard deviation	0.55	0.26	0.46	0.29

Table 2
Fatigue test results of butt-welded joint specimens made of Q345qD bridge steel.

Temperature	Specimen number	Stress range (MPa)	Fatigue life (cycle)	Failure mode
Room temperature	BW-1	270	132,952	Corner crack
	BW-2	252	507,556	Semi-elliptical crack
	BW-3	234	382,309	Multi-elliptical crack
	BW-4	216	290,029	Semi-elliptical crack
	BW-5	198	489,455	Semi-elliptical crack
	BW-6	180	487,232	Semi-elliptical crack
	BW-7	180	1,035,832	Semi-elliptical crack
	BW-8	171	2,000,000	Not failed
	BW-9	171	930,941	Multi-elliptical crack
	BW-10	162	1,286,083	Semi-elliptical crack
	BW-11	153	2,000,000	Not failed
	BW-12	153	2,000,000	Not failed
−60 °C	BWL-1	270	208,526	Semi-elliptical crack
	BWL-2	252	792,475	Semi-elliptical crack
	BWL-3	234	704,420	Multi-elliptical crack
	BWL-4	216	694,696	Multi-elliptical crack
	BWL-5	198	601,174	Semi-elliptical crack
	BWL-6	180	2,000,000	Not failed
	BWL-7	171	1,283,245	Semi-elliptical crack
	BWL-8	162	1,172,675	Semi-elliptical crack
	BWL-9	153	2,000,000	Not failed
	BWL-10	153	2,000,000	Not failed

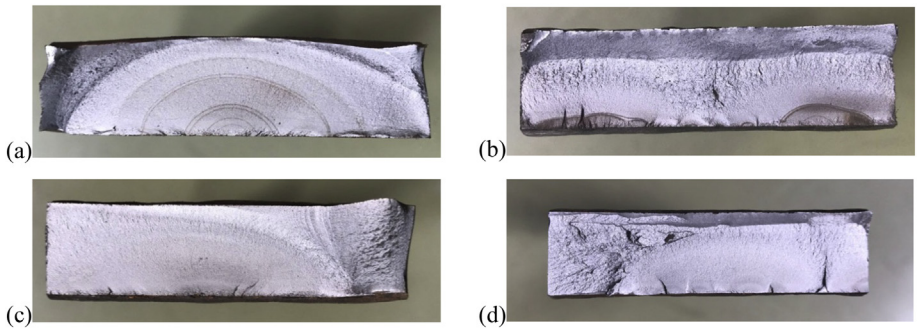

Fig. 3. Cracks on fracture surfaces in butt-welded specimens tested at RT and −60 °C (a) specimen BW-7 with single semi-elliptical crack, (b) specimen BW-3 with multiple semi-elliptical cracks, (c) specimen BWL-7 with single semi-elliptical crack, (d) specimen BWL-3 with multiple semi-elliptical cracks.

Although the test results show some scatters, together with the mean-life fitting curves, it still indicates that the fatigue life at −60 °C exhibits small improvement compared with that at RT. Fig. 5 presents the upper and lower boundaries of the test results with a survival probability level of 95% to cover the discreteness of the fatigue data. In the view of the scatter bandwidth, the fatigue life at the low temperature is higher than that at RT, indicating the low temperature do not deteriorate the fatigue strength of the butt-welded joints.

4. Fatigue life prediction using 3D crack propagation analysis

4.1. Computational procedure

LEFM is an effective tool to simulate the fatigue crack propagation of welded joints with initial defects, such as crack-like defects, inclusions, lack of fusion. This study combines the ABAQUS [30] and Franc3D [31] to conduct the LEFM-based 3D crack propagation simulation. Based on the global FE model in ABAQUS, the Franc3D inserts the initial crack, meshes and re-meshes the local FE model with tetrahedral elements, calculates the new crack front and predicts the propagation life. The following sections describe some important input parameters for Franc3D analysis complying with the observation of the fatigue test results. Since the welded details always have initial defects with detectable sizes, this study will not include the crack initiation life into the entire fatigue life of the butt-welded joints.

4.1.1. Determination of initial crack

The first step of the crack propagation analysis is to introduce the initial crack. The size, shape and location of the initial crack

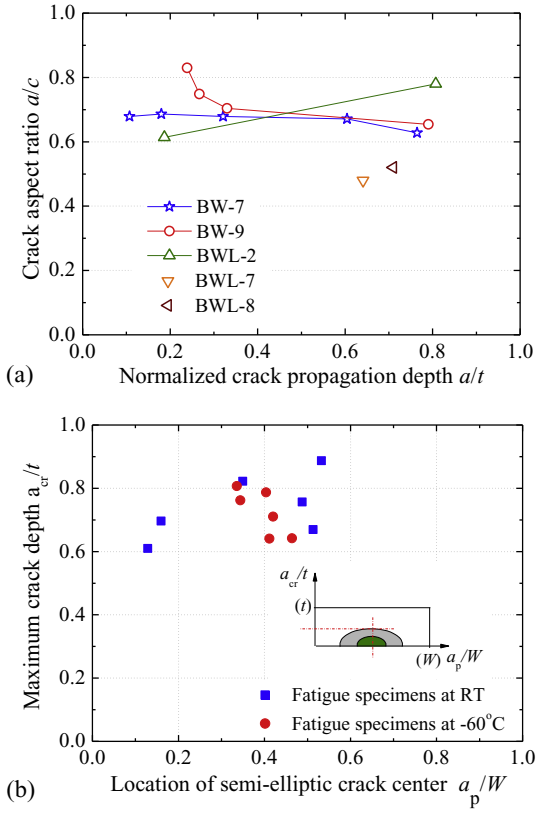

Fig. 4. Crack shape, position and depth in the fractured surfaces (a) crack aspect ratio, (b) critical crack depth versus crack center location.

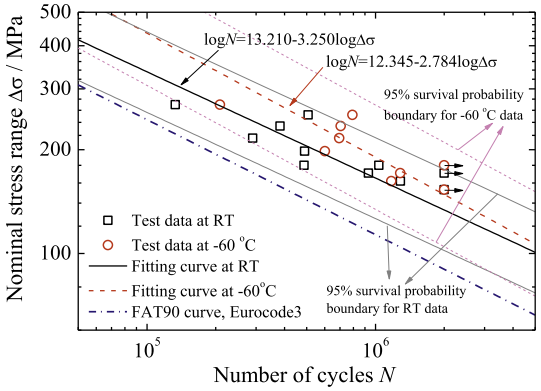

Fig. 5. Fatigue test results at RT and −60 °C.

impose some effect on the computational results. In practice, the crack initiation site is random, and the initial crack size is also changing along the welds [32,33]. This study adopts a fictitious crack depth. Nielsen & Agerskov [34] have indicated that the lower and upper boundaries of the initial crack sizes for the fatigue assessment of welded joints are 0.075 mm and 0.4 mm. Radaj et al. [35] has proposed the initial size a_0 of 0.1 mm–0.25 mm for fatigue assessment of welded structures. Lassen & Recho [36] have suggested that the LFEM is only applicable for the crack size above 0.1 mm. IIW [27] has recommended the initial size a_0 of 0.15 mm for the crack nucleated at weld toe. Therefore, this study adopts two initial crack sizes of $a_0 = 0.15$ mm and $a_0 = 0.4$ mm for the numerical fatigue crack propagation of the butt-welded joints, and the initial crack plane is parallel to the plate thickness direction along the weld toe in the base plate. According to the observation in tests, the shape of the initial crack adopts the surface semi-ellipse with the a/c of 0.7 at RT and 0.6 at −60 °C respectively. Since the distribution of the locations of initial cracks is dispersing, as shown in the Fig. 4(b), this study assumes that the initiation site for single-crack model is in the middle of the weld at toe for convenience, namely $a_p = W/2$.

4.1.2. Crack propagation analysis

This study performed the 3D mixed-mode crack propagation analysis under the constant amplitude loading condition, as the tests observed multi-crack propagation modes, and the axial tensile load would generate secondary stresses in the non-cracked sections with the increase of crack propagation depth. The equivalent SIF range ΔK_{eq} is computed instead of ΔK_I, containing a combination of two or three of the ΔK_I, ΔK_{II} and ΔK_{III}, giving in Eq. (1) [23,24].

$$\Delta K_{eq} = \sqrt{\Delta K_I^2 + \Delta K_{II}^2 + \Delta K_{III}^2/(1-\upsilon)} \tag{1}$$

where the Poisson ratio υ equals 0.3 in this study. In the event of mixed-mode condition, the crack propagation direction and kink angle do not grow along the original crack plane. It depends on the complex stress condition around the crack tips. This study adopts the Maximum Tensile Stress criterion [37] to determine the kink angel referring to the suggestion by Zong et al. [7], Aygül et al. [23], Wang et al. [24], and Blažić et al. [38]. Then, the crack propagation analysis in Franc3D should define the crack increment Δa_{median} of the crack front point with the median value ΔK_{median} for each step. The initial crack increment is specified as $\Delta a_{median} = 0.1$ mm for the first 20 steps, and then it is doubled for the each next 10 steps. The largest crack increment is 1.0 mm. The crack increment Δa_i of other crack front points is calculated following the Eq. (2) [31].

$$\Delta a_i = \Delta a_{median}\left(\frac{\frac{da}{dN_i}(\Delta K_i,\ R_i,\ldots)}{\frac{da}{dN_{median}}(\Delta K_{median}, R_{median},\ldots)}\right) \tag{2}$$

where R_i and R_{median} are the stress ratios of the cyclic load at node i and node with the median value ΔK_{median} of the crack front. Since the testing load ratio is 0.1, the cyclic load in Franc3D also adopts the same stress ratio. The fatigue life of the butt-welded specimens is determined by using the Paris law [39], shown in Eq. (3).

$$da/dN = C\bullet(\Delta K_{eq})^m \tag{3}$$

The current study defines the Paris-law parameters C and m from the fatigue crack propagation rate tests by Liao et al. [26], which used the standard compact tension specimens sampled from the same Q345qD bridge steel plates. The Paris-law parameters of the Q345qD base material derived are $C = 2.075 \times 10^{-12}$ N·mm$^{3/2}$ and $m = 2.653$ at RT, and $C = 2.432 \times 10^{-13}$ N·mm$^{3/2}$ and $m = 2.891$ at -60 °C. As test results from former researches [26,40,41] have also indicated that the fatigue crack propagation rate in base metal is higher than that in heat-affected zone and butt weld, the Paris-law parameters adopted here can be even conservative. The critical crack sizes observed in the tests define the termination of the numerical analysis for estimating the fatigue life.

4.2. FE modeling

4.2.1. Single-crack FE model

The global FE model of the butt-welded specimen without initial crack, as shown in Fig. 6(a) and (b), is built with 20-node brick elements using ABAQUS software. Table 1 lists the geometric dimensions. The boundary conditions include a fix support at one end and a pin support at the other end. A shear force is created in the surface of the clamping section to simulate the tensile loading

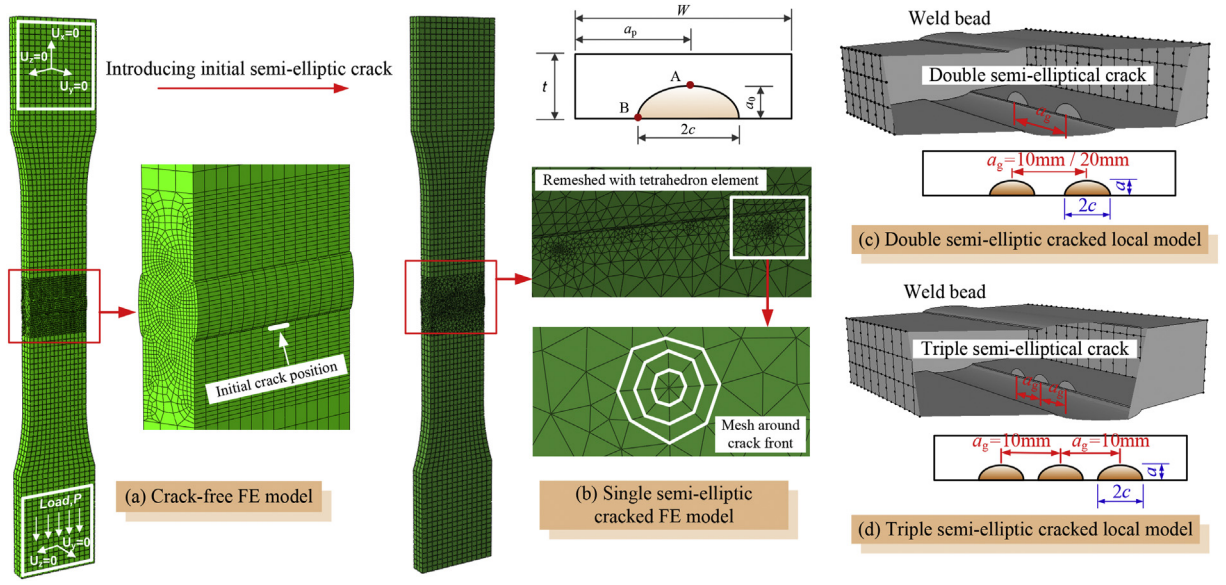

Fig. 6. FE models for the butt-welded specimen (a) global crack-free model, (b) single-crack model with a detailed crack-front mesh, (c) double-crack model, (d) triple-crack model.

exerted by the MTS machine.

After an initial semi-elliptical crack is introduced at the weld toe in base plate of the local model, Franc3D software generates the more refined meshes around the crack tip. Fig. 6(b) presents the symmetrically distributed tetrahedral elements around the crack tip, which contain three rings of elements near the entire crack front. This study adopts the linear-elastic FE analysis to compute the mixed-mode SIF with M-integral approach implemented in Franc3D [31].

4.2.2. Multi-crack FE model

From the fractured surface observation of the tested specimens, multiple initial cracks always initiate and propagate at several sites along the weld toe, and gradually merge into a bigger semi-elliptical crack. Thus, this study introduces the symmetrically arranged double semi-elliptical cracks and triple semi-elliptical cracks model as an attempt, and these multiple cracks are co-planar. Fig. 6(c) and (d) show the local FE models with multiple semi-elliptical cracks, including the double-crack model with the crack center distance a_g = 10 mm and a_g = 20 mm, and the triple-crack model with the crack center distance a_g = 10 mm. The other conditions including boundary, mesh size, and Paris-law parameters, are the same as those in the single-crack model. Due to the marginal effect of the value a/c on the predicted fatigue life mentioned in Section 3.2, the crack propagation analysis herein sets a/c = 0.5, and a_0 = 0.4 mm for FE simulation.

4.3. Numerical results and discussion

计算应力强度因子

4.3.1. Calculation of stress intensity factors

The accurate computation of the SIF is critical in the fatigue propagation life prediction using the LEFM. Fig. 7(a) validates the effectiveness of the K_I derived from 3D crack propagation analysis by comparing the maximum mode-I SIF values $K_{I,max}$ from the analytic equations in BS7910 [42] under cyclic loading. The $K_{I,max}$ values are numerically computed using the single-crack model of the butt-welded specimens with the initial semi-elliptical size a_0 = 0.4 mm under the maximum nominal tension stress of σ_{max} = 120 MPa. ~~Within the range of a = 0.4 mm to a = 6 mm, the numerical results are slightly smaller than the analytic results. For the crack size larger than 6 mm, the analytic calculations of $K_{I,max}$ are increasingly higher than the numerical results with increasing crack depth.~~

Under the applied nominal tension stress of σ_{max} = 160 MPa, Fig. 7(b) compares the $K_{I,max}$ with the corresponding equivalent SIF K_{eq} derived from the single-crack FE models at RT and −60 °C under different initial crack sizes. The difference between the $K_{I,max}$ and K_{eq} is negligible, indicating that the mode-I crack plays a dominant role in the crack propagation of butt-welded joints with a

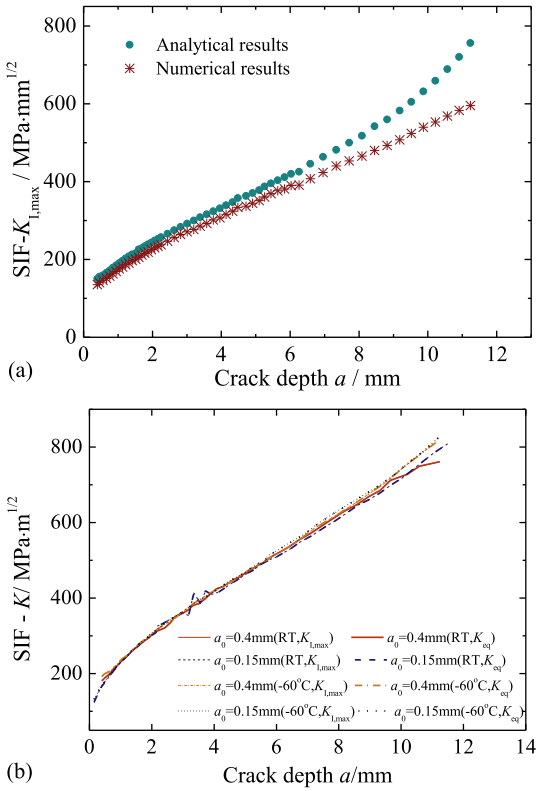

Fig. 7. Calculation of stress intensity factors using single-crack model (a) numerical results versus analytic solution, (b) numerical $K_{I,max}$ versus numerical K_{eq}.

semi-elliptical crack under tensile loading.

Fig. 8 presents the numerical results of the $K_{I,max}$ against the crack depth a under different paths, since mode-I crack dominates the fatigue crack propagation of the butt-welded joints in this study. The FE models include a single-crack, a double-crack and a triple-crack with the initial size $a_0 = 0.4$ mm. The maximum nominal tension stress σ_{max} is 140 MPa. The observed $K_{I,max}$ along the path 1, path 2, path3, and path 4, indicates that the more crack number is introduced, the higher $K_{I,max}$ is resulted. Additionally, based on the $K_{I,max}$ along the path 5, path 6, and path 7, at the sites of crack coalescence, the $K_{I,max}$ was sharply increased. This leads to a higher crack propagation rate to facilitate the newly-merging crack evolving into a larger semi-elliptical crack. As the crack propagation rate is already greatly accelerated when the adjacent cracks are about to coalesce for the cases in this study, the SIF indicator used would underestimate the near-tip stress field of the adjacent cracks without considering the crack interaction effect [43], but could marginally affect the numerical fatigue life with multiple cracks. The crack propagation tracks in Fig. 8 also illustrate that the 3D crack propagation analysis provides a new way to simulate the crack track for both of the single-crack and multiple-crack conditions.

4.3.2. Comparison of the predicted and experimental fatigue life

Fig. 9 presents the prediction S–N curves of the butt-welded specimens using the single-crack model with the initial size $a_0 = 0.15$ mm and $a_0 = 0.4$ mm. As shown in Fig. 9(a), the crack propagation analysis with both initial crack sizes predicts the fatigue life of the specimens in good agreement with the test data at RT. Predicted results with $a_0 = 0.15$ mm can almost approach the median curve of the test data. As shown in Fig. 9(b), the FE model with $a_0 = 0.4$ mm achieves a better prediction and almost coincides with the experimental fitting curve at −60 °C, while the predicted fatigue life with $a_0 = 0.15$ mm is generally higher than the median curve of the test results. Overall, the 3D crack propagation analysis with $a_0 = 0.4$ mm can provide a good prediction of the fatigue life of the studied joints at both RT and −60 °C.

Fig. 10(a) and (b) compares the prediction fatigue life of the butt-welded specimens based on the single, double and triple semi-elliptical crack models with initial size $a_0 = 0.4$ mm at RT and −60 °C. The multiple-crack models predict slightly conservative fatigue lives compared with the single-crack model, although the differences are marginal. More initial cracks in the FE model lead to a more conservative prediction value. Additionally, for the double-crack models, the effect due to the distances between different crack centers is negligible on the prediction fatigue life. The relative large values of a_g/a_0 may explain this minor effect, which is in accordance with the results of Seah & Qian [43]. The predicted fatigue strengths at 2 million cycles $\Delta\sigma_C$ of the studied specimens based on the single, double and triple crack model at RT are 110 MPa, 102 MPa, 100 MPa, and 96 MPa, while those at −60 °C are 146 MPa, 137 MPa, 133 MPa, and 128 MPa, respectively. The predicted fatigue life derived from the triple-crack model is obviously lower than that from the single-crack model, and the fatigue strength derived from the 3D crack propagation analysis at −60 °C obviously exceeds that at RT.

4.4. Effect of low temperature on fatigue life

4.4.1. Paris-law parameters

Within the range of the RT to −60 °C, previous investigations [9,26,44] have experimentally confirmed that the low temperature decreases the fatigue crack propagation rate of the low-alloy steels indexed by the Paris-law parameters C and m. This finding is applicable to the Q345qD bridge steel in this study. Based on the 3D single-crack propagation analysis using different Paris-law parameters, Fig. 11 compares the single-crack prediction results of the fatigue life of the investigated joints at RT and −60 °C with the initial semi-elliptical crack size $a_0 = 0.4$ mm. The recommended S–N curve by Eurocode3 [3] lies below the predicted S–N curve at RT, and the prediction life at −60 °C is obviously higher than that at RT. The enhanced resistance to the fatigue crack propagation of the bridge steel may explain the improved fatigue properties of the butt-welded joints at −60 °C.

4.4.2. Reduced fracture toughness

It is well known that the low temperature reduces the fracture toughness of the steel materials, leading to a reduced critical crack

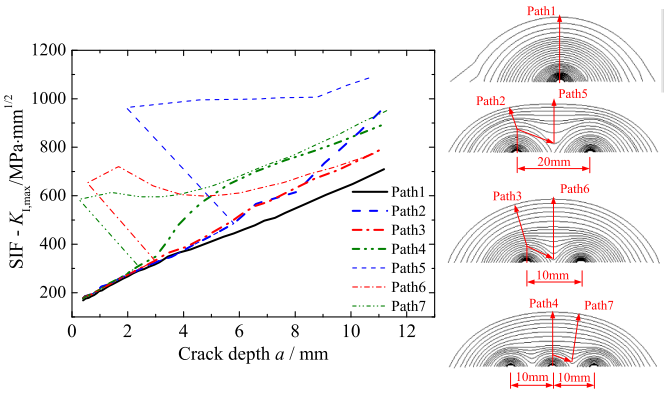

Fig. 8. Comparison of $K_{I,max}$ derived from single-crack model and multiple-crack model.

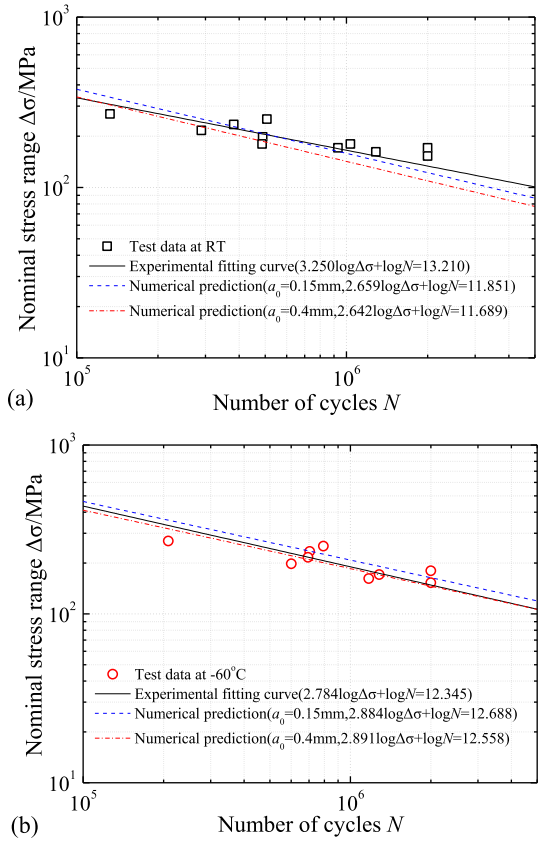

Fig. 9. Predicted *S-N* curves using the single-crack model (a) at RT, (b) at −60 °C.

size [42,44]. Thus, this section investigated the effect of the reduced critical crack size on the fatigue life of butt-welded joints based on the 3D crack propagation analysis. The bridge steel Q345qD is with a relatively high fracture toughness K_{IC} [42], but the K_{IC} is hard to be experimentally obtained. BS7910 [42] recommends deriving the fracture toughness K_{IC} from the tested Charpy impact energy A_{KV}. Based on the test results of A_{KV} by Liao et al. [26] and equations given by BS7910 [42] Annex J.2, Fig. 12(a) presents the estimated K_{IC} values of Q345qD bridge steel plate with a thickness of 16 mm against the reduced temperatures. The K_{IC} at RT is about 4500 MPa·m$^{1/2}$, while the K_{IC} drops to around 1600 MPa·m$^{1/2}$ at −60 °C.

Fig. 12(b) explains the effect of the reduced K_{IC} on the fatigue life in the studied joints with an initial semi-elliptical crack size a_0 = 0.4 mm under the cyclic loading with the maximum nominal tension stress σ_{max} of 120 MPa. The K_I at the deepest point of the crack tip has not reached the 1620 MPa·m$^{1/2}$ even that the crack almost penetrate the plate, which means the reduced K_{IC} values do not introduce premature fracture, similar to the reports by Schilling et al. [45]. The fatigue life at −60 °C is generally higher than that at RT. In addition, after the crack depth exceeds the half of the plate thickness, the fatigue crack propagation rates at both RT and −60 °C are already very high, contributing negligibly to the fatigue propagation life. It demonstrates that the reduced critical crack depth due to the declined fracture toughness poses a marginal effect the fatigue life of the butt-welded joints at low temperatures.

5. Conclusion

This study investigates the fatigue properties of the butt-welded joints at RT and −60 °C by means of constant amplitude fatigue tests and 3D crack propagation analysis. The above investigation supports the following observations and conclusions:

(1) The fatigue life of butt-welded joints at low temperatures will not be lower than that at RT, and the contrast fatigue data at RT and −60 °C presented in this study provide an important reference for the engineering practice. The welding procedure and Q345qD bridge steel utilized here is applicable to welded joints in the cold and sever cold regions.
(2) The improvement of the fatigue properties of the butt-welded joints probably attributes to the enhanced resistance to the fatigue crack propagation of the steel materials, since all the crack initiation and propagation always occur in the base material along the weld toe.
(3) Since the Q345qD bridge steel already possesses relatively higher fracture toughness, the reduced fracture toughness or the reduced critical crack size affects negligibly the fatigue life of the butt-welded joints at low temperatures.
(4) The 3D crack propagation analyses of the FE model with the initial crack size a_0 = 0.15 mm–0.4 mm realize a good prediction of

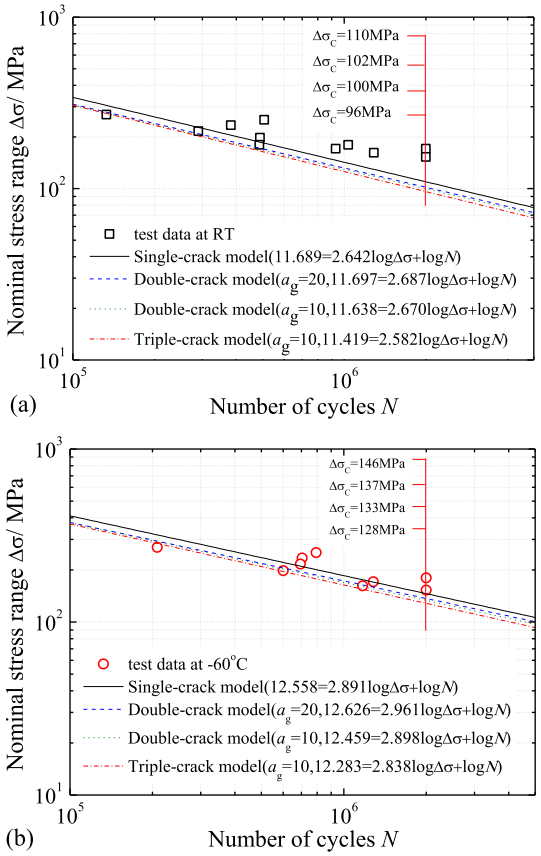

Fig. 10. Predicted *S-N* curves using the multiple-crack model (a) at RT, (b) at −60 °C.

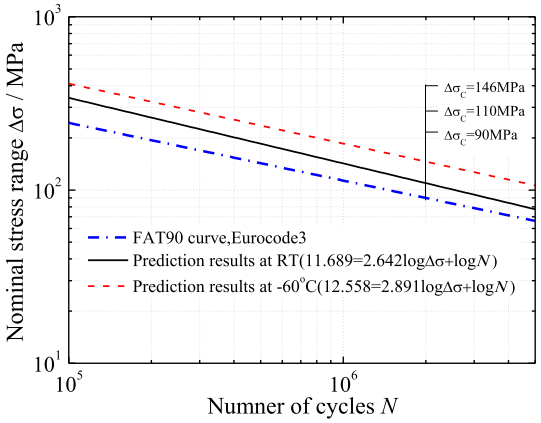

Fig. 11. Effect of temperature-dependent Paris-law parameters *C* and *m* on the prediction life of butt-welded specimens.

the fatigue life for the butt-welded joints in this study. The mode-I SIF K_I dominates the crack propagation behavior in butt-welded joints under cyclic tension loading.

(5) The utilization of the multiple-crack model in the 3D crack propagation analysis in this paper proposes a more accurate way for the fatigue crack propagation simulation of fatigue details, since the initial cracks always nucleate at several sites simultaneously for the welded joints.

6. Recommendations for future work

This study recommends extending the current results by further fatigue test validation of butt-welded joints under variable

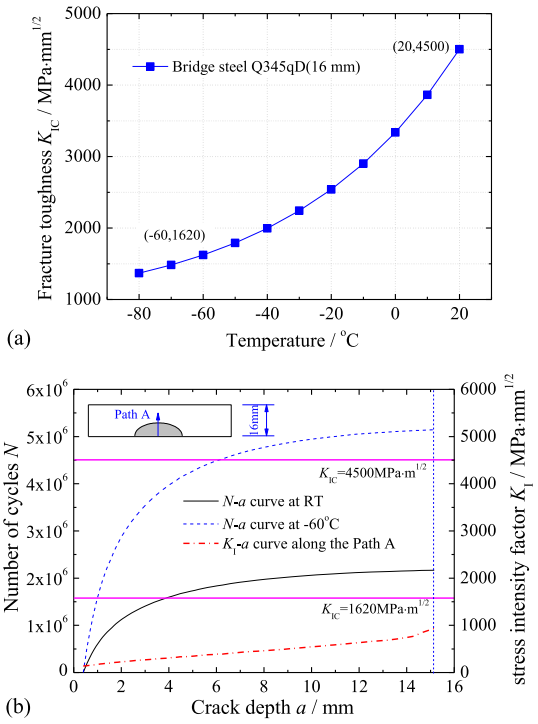

Fig. 12. Effect of reduced fracture toughness on fatigue crack propagation life of butt-welded specimens (a) estimated K_{IC} of Q345qD bridge steel, (b) effect of reduced K_{IC} on fatigue life.

amplitude loading at a low ambient temperature, since the realistic vehicle actions encompass diverse loading sequences and stress ranges. The different loading blocks with the effect of low temperatures probably lead to different crack propagation behavior and fatigue life.

In addition, the measurement and numerical simulation of the distribution of welding residual stresses are also recommended for future work to achieve more accurate and realistic 3D crack propagation analyses of welded joints, as the tensile residual stresses would accelerate the fatigue crack propagation rates around the weld toes. In addition, the multi-crack simulation needs more experimental validation after its feasible attempt in this study, and the corresponding computation of the fatigue crack propagation life should also consider the co-planar crack interaction effect in the further investigation.

Declarations of Competing Interest

None.

Acknowledgements

This work was supported by the National Natural Science Foundation of China (Grant Nos. 51378289 and 51678339) and the China Postdoctoral Science Foundation (Grant No. 2018M630164). The support on the authorization of the Franc3D software by Mr. Mengguang Li in MVT GROUP INC. was also gratefully acknowledged.

References

[1] Y.Q. Wang, Survey of investigation about brittle fracture of steel structure under low temperature, Steel Constr. 9 (1994) 217–221 (in Chinese).
[2] TB 10091, Code for Design on Steel Structures of Railway Bridge, (2017) (in Chinese).
[3] Eurocode3, Design of steel structures-Part1–9: fatigue, (2005).
[4] American Association of State Highway and Transportation Officials, AASHTO LRFD Bridge Design Specification, (2007).
[5] I. Lillemäe, H. Lammi, L. Molter, H. Remes, Fatigue strength of welded butt joints in thin and slender specimens, Int. J. Fatigue 44 (2012) 98–106.
[6] G.K. Ahiale, Y.J. Oh, Microstructure and fatigue performance of butt-welded joints in advanced high-strength steels, Mat. Sci. Eng. A 597 (2014) 342–348.
[7] L. Zong, G. Shi, Y.Q. Wang, Z.X. Li, Y. Ding, Experimental and numerical investigation on fatigue performance of non-load-carrying fillet welded joints, J. Constr. Steel Res. 130 (2017) 193–201.
[8] L.Y. Feng, X.D. Qian, A hot-spot energy indicator of welded plate connections under cyclic axial loading and bending, Eng. Struct. 147 (2017) 598–612.
[9] R.I. Stephens, J.H. Chung, G. Glinka, Low temperature fatigue behavior of steels- a review, 39th Annual Earthmoving Industry Conference, 1979.
[10] L. Ma, J. Guo, Q.Y. Liu, W.J. Wang, Fatigue crack growth and damage characteristics of high-speed rail at low ambient temperature, Eng. Fail. Anal. 82 (2017) 802–815.
[11] O.H. Ibrahim, I.S. Ibrahim, T.A.F. Khalifa, Impact behavior of different stainless steel weldments at low temperatures, Eng. Fail. Anal. 17 (5) (2010) 1069–1076.

[12] Y.Q. Wang, X.W. Liao, D.F. Jia, Y.J. Shi, Overview of research progress for the low-temperature fatigue performance of steel structures, Progr. Steel Build. Struct. 20 (1) (2018) 1–11 (in Chinese).
[13] X.L. Jia, W.T. Liu, P-S-N curve of fatigue at low temperatures of welded components, J. Beijing Univ. Aeronautics Astronautics 27 (6) (2001) 684–686 (in Chinese).
[14] Shul'ginov B S, V.V. Matveyev, Impact fatigue of low-alloy steels and their welded joints at low temperature, Int. J. Fatigue 19 (8–9) (1997) 621–627.
[15] K.W. Kang, B.C. Goo, J.H. Kim, D.K. Kim, J.K. Kim, Experimental investigation on static and fatigue behavior of welded SM490A steel under low temperature, Int. J. Steel Struct. 9 (2009) 85–91.
[16] D.J. Jeong, T. Park, J. Lee, S. Kim, Ambient and cryogenic S-N fatigue behavior of Fe15Mn steel and its weld, Met. Mater. Int. 21 (3) (2015) 453–460.
[17] D. Bowness, M.M.K. Lee, Weld toe magnification factors for semi-elliptical cracks in T-butt joints – comparison with existing solutions, Int. J. Fatigue 22 (5) (2000) 389–396.
[18] S.T. Lie, S.P. Vipin, T. Li, New weld toe magnification factors for semi-elliptical cracks in double-sided T-butt joints and cruciform X-Joints, Int. J. Fatigue 80 (2015) 178–191.
[19] T. Nykänen, X.Y. Li, Y. Björk, G. Marquis, A parametric fracture mechanics study of welded joints with toe cracks and lack of penetration, Eng. Fract. Mech. 72 (2005) 1580–1609.
[20] Z. Barsoum, B. Jonsson, Fatigue assessment and LEFM analysis of cruciform joints fabricated with different welding processes, Weld World 52 (7–8) (2008) 93–105.
[21] To S, S.B. Lambert, D.J. Burns, A multiple crack model for fatigue in welded joints, Int. J. Fatigue 15 (4) (1993) 333–340.
[22] X.D. Qian, C.T. Nguyen, Y. Petchdemaneengam, Z.Y. Ou, S. Swaddiwudhipong, P. Marshall, Fatigue performance of tubular X-joints with PJP + welds: II - numerical investigation, J. Constr. Steel Res. 89 (2013) 252–261.
[23] M. Aygül, M. Al-Emrani, Z. Barsoum, J. Leander, Investigation of distortion-induced fatigue cracked welded details using 3D crack propagation analysis, Int. J. Fatigue 64 (2014) 54–66.
[24] Z.Y. Wang, Y.F. Zhang, Y.Q. Wang, X.X. Du, H.X. Yuan, Numerical study on fatigue behavior of tubular joints for signal support structures, J. Constr. Steel Res. 143 (2018) 1–10.
[25] GB 50661, Code for Welding of Steel Structures, (2011) (in Chinese).
[26] X.W. Liao, Y.Q. Wang, X.D. Qian, Y.J. Shi, Fatigue crack propagation for Q345qD bridge steel and its butt weld at low temperatures, Fatigue Fract. Eng. Mater. Struct. 41 (2018) 675–687.
[27] A. Hobbacher, Recommendations for Fatigue Design of Welded Joints and Components, Springer International Publishing, Cham, 2016.
[28] J. Leander, M. Aygül, B. Norlin, Refined fatigue assessment of joints with welded in-plane attachments by LEFM, Int. J. Fatigue 56 (2013) 25–32.
[29] D.H. Choi, H.Y. Choi, D. Lee, Fatigue life prediction of in-plane gusset welded joints using strain energy density factor approach, Theor. Appl. Fract. Mec. 45 (2) (2006) 108–116.
[30] M. Hibbit, J. Karlsson, R.I. Pawtucket, ABAQUS/Standard User's Manual, Version 6.5, Simulia, Providence, RI, 2005.
[31] Franc3D, Reference Manual for Version 7, Fracture Analysis Consultants Inc., 2016.
[32] Y.H. Zhang, S.J. Maddox, Fatigue life prediction for toe ground welded joints, Int. J. Fatigue 31 (2009) 1124–1136.
[33] S. Beretta, A. Bernasconi, M. Carboni, Fatigue assessment of root failures in HSLA steel welded joints: a comparison among local approaches, Int. J. Fatigue 31 (2009) 102–110.
[34] J.A. Nielsen, H. Agerskov, Fatigue in steel highway bridges under random loading, J. Struct. Eng. 125 (2) (1999) 152–162.
[35] D. Radaj, C.M. Sonsino, W. Fricke, Fatigue Assessment of Welded Joints by Local Approaches, Woodhead Publishing Limited, Cambridge, 2006.
[36] T. Lassen, N. Recho, Proposal for a more accurate physically based S-N curve for welded steel joints, Int. J. Fatigue 31 (1) (2009) 70–78.
[37] F. Erdogan, G.C. Sih, On the crack extension in plates under plane loading and transverse shear, J. Basic Eng. 85 (4) (1963) 519–525.
[38] M. Blažić, S.M. Maksimović, Z. Petrović, I. Vasović, D. Turnić, Determination of fatigue crack growth trajectory and residual life under mixed modes, J. Mech. Eng. 60 (4) (2014) 250–254.
[39] P. Paris, F. Erdogan, A critical analysis of crack propagation laws, J. Basic Eng. 85 (4) (1963) 528–533.
[40] Y. Xiong, X.X. Hu, The effect of microstructures on fatigue crack growth in Q345 steel welded joint, Fatigue Fract. Eng. Mater. Struct. 35 (2012) 500–512.
[41] E.L. Pautremat, C. Vallet, Low temperature fatigue behavior of E355 grade RAD steel welded joints, Weld. Int. 11 (4) (1997) 283–294.
[42] BS1910, Guide to Methods for Assessing the Acceptability of Flaws in Metallic Structures, (2005).
[43] T.T. Seah, X.D. Qian, An interaction factor to estimate the over-constraining effect in plates with co-planar cracks, Eng. Fract. Mech. 199 (2018) 13–28.
[44] C.L. Walters, A. Alvaro, J. Maljaars, The effect of low temperatures on the fatigue crack growth of S460 structural steel, Int. J. Fatigue 82 (2016) 110–118.
[45] C.G. Schilling, K.H. Klippstein, J.M. Barsom, S.R. Novak, G.T. Blake, Low temperature tests on simulated bridge members, J. Struct. Div. 101 (ST1) (1975) 31–48.